**RAA 2017** Vol. **17** No. **11**, 117 (10pp) doi: 10.1088/1674–4527/17/11/117

*http://www.raa-journal.org* *http://iopscience.iop.org/raa*

***R**esearch in*
***A**stronomy and*
***A**strophysics*

# Elliptical distortion of the Milky Way's rotation traced by high-mass star-forming regions

Ping-Jie Ding[1,2], Zi Zhu[1,2] and Jia-Cheng Liu[1,2]

[1] School of Astronomy and Space Science, Nanjing University, Nanjing 210023, China; *zhuzi@nju.edu.cn*
[2] Key Laboratory of Modern Astronomy and Astrophysics (Nanjing University), Ministry of Education, Nanjing 210023, China

Received 2017 February 27; accepted 2017 August 16

**Abstract** The gravitational potential of the Milky Way is non-axisymmetric, caused by a bar or triaxial halo, which dominates elliptical rotation of the Milky Way. Employing a likelihood analysis, we exploit the astrometric data of masers thoroughly and constrain the elliptical rotation of the Galaxy. Masers in high-mass star-forming regions, observed by VLBA, are more distant tracers than stars observed in the optical bandpass, and thus are more appropriate for studying the global feature of the Milky Way's rotation. A clear elliptical potential of the Milky Way is detected, with an ellipticity of $\epsilon_0 \sim 0.09$ at the Sun, and the ellipticity increases towards the outer disk. The minor axis of the elliptical potential (the major axis of the rotation orbit) is found to be near the Sun with a displacement of $\sim 32^\circ$. Based on the rotation model assumed for an elliptical potential, we also make a kinematical calibration of the Galactocentric distance of the Sun, which gives $R_0 = 7.63 \pm 0.34\,\mathrm{kpc}$.

**Key words:** astrometry — Galaxy: fundamental parameters — Galaxy: kinematics and dynamics — methods: data analysis

## 1 INTRODUCTION

The rotation feature of the Milky Way remains uncertain due to the limit of observations and the choice of models. The estimate of rotation speed at the location of the Sun varies from around $200\,\mathrm{km\,s^{-1}}$ to $\gtrsim 260\,\mathrm{km\,s^{-1}}$ (Elias et al. 2006; Zhu 2006; McMillan & Binney 2010; Reid et al. 2014; Sharma et al. 2014; Bobylev & Bajkova 2015b; Bobylev & Bajkova 2017) relying on different samples and methodologies. The rotation curve is found to be nearly flat in the solar neighborhood with a slight inclination (Uemura et al. 2000; Zhu 2006; López-Corredoira 2014; Huang et al. 2016) but the global feature of the rotation curve is still under debate (McMillan & Binney 2010; Chemin et al. 2015; Reid & Dame 2016). Traditionally the Milky Way's rotation is proposed to be circular. However, it has been found that some large-scale non-axisymmetric structures such as a bar in the central few kpc of the disk and a triaxial halo exist in the Galaxy (de Vaucouleurs 1970; Dwek et al. 1995; Rojas-Niño et al. 2015; Gerhard 2016), which can notably impact the shape of Galactic rotation (Binney 1978; Blitz & Spergel 1991; Kuijken & Tremaine 1994; Kuijken 1996; Chemin et al. 2015). In this circumstance, a circular rotation model could be insufficient for describing the rotation of our home galaxy.

In the work of Kuijken & Tremaine (1994) (hereafter KT94), the authors formulated a non-axisymmetric model for describing the Milky Way's elliptical rotation and investigated the ellipticity of the rotation orbit using data on HI gas, distant carbon stars, Cepheids and HII regions. They pointed out that the Sun lies near the minor axis of the Galaxy's elliptical potential. Metzger et al. (1998) adopted 288 Cepheids to probe the non-axisymmetry of the disk based on the KT94 model and found the antisymmetric component of the rotation ellipticity to be $s_0 = 0.043 \pm 0.016$ near the Sun, together with an estimate of $R_0 = 7.66 \pm 0.32\,\mathrm{kpc}$ for

the Galactocentric distance of the Sun. Moreover, using nearly 300 open clusters within a range of 3 kpc from the Sun, Zhu (2008) found a potential ellipticity $\epsilon_0 \sim 0.048 - 0.066$ and a displacement of the Sun from the minor axis of the potential around $30^\circ$. Some other research has also suggested that stellar kinematics in the solar neighborhood could reveal some non-axisymmetry in Galactic rotation (Bovy et al. 2012; López-Corredoira & González-Fernández 2016).

The reliability of the measured Galactic parameters improves with both the spatial coverage of tracers and observation precision. The data of maser sources in high-mass star-forming regions (HMSFRs) are most appropriate for analyzing the non-axisymmetry in the Milky Way's rotation, since masers are young and bright sources widely spread over the disk (extending out to $> 8\,\mathrm{kpc}$ from the Sun). The Bar and Spiral Structure legacy (BeSSeL) Survey and the Japanese VLBI Exploration of Radio Astrometry (VERA) have yielded more than 100 astrometric measurements of maser sources associated with HMSFRs. The typical accuracy of the measured parallaxes is $\sim 20\,\mu\mathrm{as}$ (Reid 2012). The first data release of the ongoing *Gaia* mission, by contrast, has announced a systematic error in parallaxes at a level of $\pm 0.3\,\mathrm{mas}$ (Lindegren et al. 2016), leading to a large uncertainty in the distance of stars far away from the Sun. In this circumstance, the maser data provide the best sample for research on the Milky Way's rotation in a large spatial coverage at this stage. In this work, we investigate Galactic kinematics using the maser data given by Reid et al. (2014). Using the maximum-likelihood (ML) method presented in Aghajani & Lindegren (2013) (hereafter AL13), we develop a likelihood analysis to exploit data and analyze the elliptical Milky Way's rotation based on the KT94 model. We also make a kinematical calibration of the Galactocentric distance of the Sun.

Section 2 lays out the data sampling. In Section 3, we introduce the KT94 model and the likelihood analysis used in our work. Our results are provided in Section 4. We discuss the results in Section 5.

## 2 DATA SAMPLE

The data used in our work are selected from 103 masers listed in table 1 of Reid et al. (2014), which consist of measurements of positions, parallaxes, proper motions and line-of-sight velocities in the local standard of rest (LSR), $v_{\mathrm{LSR}}$, associated with the observational uncertainties. The LSR is defined based on the standard solar motion $(U_\odot^{\mathrm{Std}}, V_\odot^{\mathrm{Std}}, W_\odot^{\mathrm{Std}}) = (10, 15, 7)\,\mathrm{km\,s^{-1}}$ (Reid et al. 2014) in the heliocentric Cartesian coordinate system such that the $u$-axis points to the Galactic center (GC), $v$-axis to Galactic transverse rotation and $w$-axis to the North Galactic Pole. The heliocentric line-of-sight velocity $\tilde{v}_r$ is recovered from $v_{\mathrm{LSR}}$.

The criterion of data selection is based on parallax errors. We reject sources with $\sigma_p/\tilde{p} \geq 0.1$ or $\sigma_p/\tilde{p}^2 \geq 0.5\,\mathrm{kpc}$. $\tilde{p}$ and $\sigma_p$ are the observed parallax and corresponding observational uncertainty. The second criterion is set to avoid a few distant sources with large uncertainties in their distances even though their relative parallax errors are $< 0.1''$. We obtain a sample including 70 maser sources that meet the above criterion. Figure 1 shows the locations of the selected maser sources projected onto the Galactic plane. The main three spiral arms (i.e. Sagittarius, Local and Perseus) are plotted in colors.

## 3 METHODOLOGY

In this section we introduce the analytic framework used to describe the Galactic kinematics. The stellar motions consist of two components: rotation velocity following the rotation curve and peculiar motion. We employ and generalize the ML method presented in AL13 to estimate the best-fitting Galactic parameters from the parallaxes, proper motions and heliocentric line-of-sight velocities of maser sources, taking into consideration observational uncertainties.

In our analysis we introduce a Galactocentric cylindrical coordinate system $(R,\, \phi,\, z)$ such that $R$ is the Galactocentric radius, the $z$ axis points to the North Galactic Pole from the GC and the azimuthal angle $\phi$ is measured in the direction of Galactic rotation.

### 3.1 Non-Axisymmetric Rotation Model

The constraint on the shape of the rotation is based on the model described in KT94. The rotation curve is produced by a primarily axisymmetric potential coupled with a small non-axisymmetric potential. The total potential is written as

$$\Psi(R,\, \phi) = \Psi_0(R) + \psi(R) \cos 2(\phi - \phi_b). \qquad (1)$$

The axisymmetric part of the potential is a power-law in Galactocentric radius proposed by KT94

$$\Psi_0(R) = \begin{cases} \frac{V_0^2}{2\alpha}\left(\frac{R}{R_0}\right)^{2\alpha} & \alpha \neq 0 \\ V_0^2 \ln(R) & \alpha = 0 \end{cases}, \qquad (2)$$

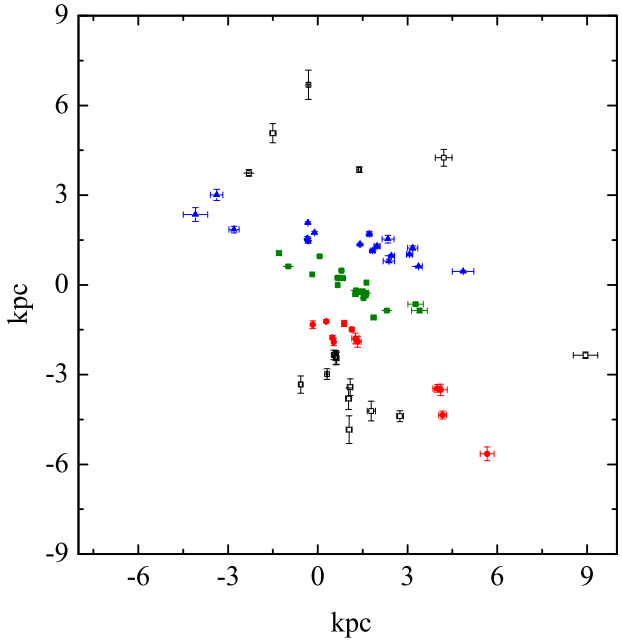


**Fig. 1** Locations of the selected maser sources projected on the Galactic plane. The Sun is located at $(0,\ 0)$. The horizontal coordinate increases towards the direction of Galactic rotation and the vertical coordinate increases towards the Galactic anticenter. The *red circles*, *olive squares* and *blue triangles* represent sources residing in the Sagittarius, Local and Perseus Arms respectively. The *black squares* signify sources located in other regions.

where $R_0$ is the Galactocentric distance of the Sun and $V_0$ the circular speed at the solar position. The non-axisymmetric part of the potential in the KT94 model is also power-law dependent on radius

$$\psi(R) = \psi_0 \left(\frac{R}{R_0}\right)^p,\ \psi_0 \geq 0. \tag{3}$$

The equipotential surfaces are approximately elliptical with axis ratio $q$. Setting $V_c(R)$ to be the circular velocity dominated by the axisymmetric part of the potential, the potential ellipticity $\epsilon$ is defined as $\epsilon(R) = 2\psi(R)/V_c(R)^2$, which is used to parameterize the non-axisymmetry of the rotation orbit. The relationship between $\epsilon$ and $q$ is $\epsilon \backsimeq 1 - q$ to first order. The parameter $\phi_b$ in Equation (1) denotes the direction of the minor axis of the potential (i.e. the major axis of the orbit). The circular velocity and potential ellipticity at any radius $R$ have the forms

$$V_c(R) = V_0 \left(\frac{R}{R_0}\right)^\alpha;\ \epsilon(R) = \epsilon_0 \left(\frac{R}{R_0}\right)^{p-2\alpha}, \tag{4}$$

and the rotation curve is given by

$$\begin{aligned} \bar{v}_R &= -\beta_1 V_c(R)\epsilon(R)\sin 2(\phi - \phi_b), \\ \bar{v}_\phi &= V_c(R) - \beta_2 V_c(R)\epsilon(R)\cos 2(\phi - \phi_b), \\ \bar{v}_z &= 0. \end{aligned} \tag{5}$$

The coefficients $\beta_1$ and $\beta_2$ are defined as

$$\beta_1 \equiv \frac{1 + p/2}{1 - \alpha},\ \beta_2 \equiv \frac{1 + p(1+\alpha)/4}{1 - \alpha}. \tag{6}$$

The KT94 model also gives the definitions of two orthogonal terms describing the ellipticity

$$s_0 = \epsilon_0 \sin 2\phi_b, \qquad c_0 = \epsilon_0 \cos 2\phi_b, \tag{7}$$

which represent the antisymmetric and symmetric components of the ellipticity about the $\phi = 0°$ line.

### 3.2 The Maximum-Likelihood (ML) Estimation

The ML method formulated by AL13 is used to fully exploit the data when observational uncertainties cannot be ignored. The authors of AL13 used the ML method to analyze local kinematics when only parallaxes and proper motions are known. In this work we employ and generalize the AL13 method by introducing the measured line-of-sight velocities and the rotation curves. The observables include parallax $\tilde{p}$, proper motions in the directions of increasing Galactic coordinates $l$ and $b$, i.e. $\tilde{\mu}_l$ and $\tilde{\mu}_b$ respectively, and the line-of-sight velocity $\tilde{v}_r$. Given the kinematical parameters $\boldsymbol{\theta} = (R_0,\ V_0,\ s_0,\ c_0,\ \boldsymbol{v}_\odot)$ (where $\boldsymbol{v}_\odot = (U_\odot,\ V_\odot,\ W_\odot)$ is the solar peculiar ve-

locity), the velocity dispersion tensor $\boldsymbol{D}$ and the observables, the log-likelihood function of one source is

$$L(\boldsymbol{\theta}, \boldsymbol{D}, p) = \ln f_{\tilde{\boldsymbol{v}}}(\tilde{\boldsymbol{v}}|p) + \ln g(\tilde{p} - p), \tag{8}$$

where $f_{\tilde{\boldsymbol{v}}}$ is the probability density function (pdf) of the observed heliocentric velocity $\tilde{\boldsymbol{v}} = (k\tilde{\mu}_l/p,\, k\tilde{\mu}_b/p,\, \tilde{v}_r)$ when the true parallax $p$ is known and $g$ is the centered normal pdf with standard deviation $\sigma_p$. The constant $k = 4.74047$ if the units for velocities, proper motions and parallaxes are $\mathrm{km\ s^{-1}}$, $\mathrm{mas\ yr^{-1}}$ and $\mathrm{mas}$ respectively.

We now need an explicit expression for the conditional pdf $f_{\tilde{\boldsymbol{v}}}(\tilde{\boldsymbol{v}}|p)$. The expected value of $\tilde{\boldsymbol{v}}$, i.e. $\boldsymbol{v}$, is deduced from the rotation curve and $\boldsymbol{v}_\odot$ (see Appendix). The dispersion tensor is defined as $\boldsymbol{D} = \mathrm{diag}(\sigma_\mathrm{R}^2, \sigma_\phi^2, \sigma_\mathrm{z}^2)$, which parameterizes the effect of stellar peculiar motions relative to the expected motion modeled by the rotation curve. In this work we set $\sigma_R = \sigma_\phi = \sigma_z \equiv \Delta$ under the assumption that the random component of stellar velocities is isotropous and satisfactorily follows a Gaussian distribution (McMillan & Binney 2010). The total covariance of $\tilde{\boldsymbol{v}}$ is the sum of $\boldsymbol{D}_{\boldsymbol{v}}$ (the covariance due to the dispersion tensor, see Appendix) and the covariance due to observational uncertainties

$$\boldsymbol{C}_{\tilde{\boldsymbol{v}}} = \boldsymbol{D}_{\boldsymbol{v}} + \begin{pmatrix} k^2\sigma_{\mu_l}^2/p^2 & k^2\rho\sigma_{\mu_l}\sigma_{\mu_b}/p^2 & 0 \\ k^2\rho\sigma_{\mu_l}\sigma_{\mu_b}/p^2 & k^2\sigma_{\mu_b}^2/p^2 & 0 \\ 0 & 0 & \sigma_{v_r}^2 \end{pmatrix}, \tag{9}$$

where $\sigma_{\mu_l}$, $\sigma_{\mu_b}$ and $\sigma_{v_r}$ are the observational uncertainties in $\mu_l$, $\mu_b$ and $v_r$ respectively, and $\rho$ the correlation coefficient between $\mu_l$ and $\mu_b$. For the simplest case both the distribution of velocity dispersion and the observational errors are Gaussian. Thus the expression of $f_{\tilde{\boldsymbol{v}}}(\tilde{\boldsymbol{v}}|p)$ can be written as

$$\begin{aligned} f_{\tilde{\boldsymbol{v}}}(\tilde{\boldsymbol{v}}|p) = {} & (2\pi)^{-\frac{3}{2}} |\boldsymbol{C}_{\tilde{\boldsymbol{v}}}|^{-\frac{1}{2}} \\ & \times \exp\left[-\frac{1}{2}(\tilde{\boldsymbol{v}} - \boldsymbol{v})^{\mathrm{T}} \boldsymbol{C}_{\tilde{\boldsymbol{v}}}{}^{-1} (\tilde{\boldsymbol{v}} - \boldsymbol{v})\right]. \end{aligned} \tag{10}$$

Now we return to Equation (8) to solve the kinematical parameters with the ML method. The log-likelihood function $L$ depends on both the kinematical parameters and the parallax $p$. We use the approximate solution formulated by AL13 to eliminate $p$ in Equation (8), and the expression of the likelihood function is simplified as

$$L(\boldsymbol{\theta}, \boldsymbol{D}) \simeq \ln f_{\tilde{\boldsymbol{v}}}(\tilde{\boldsymbol{v}}|\tilde{p}) + \frac{1}{2}\sigma_p^2 F^2(\tilde{p}), \tag{11}$$

where $F(\tilde{p}) = \left(\partial \ln f_{\tilde{\boldsymbol{v}}}(\tilde{\boldsymbol{v}}|p)/\partial p\right)_{p=\tilde{p}}$. This is the log-likelihood expression for one source and the total log-likelihood function used for all the sources should be written as

$$L(\boldsymbol{\theta}, \boldsymbol{D}) \simeq \sum_{i=1}^{N} \left[ f_{\tilde{\boldsymbol{v}},i}(\tilde{\boldsymbol{v}}_i|\boldsymbol{\theta}, \boldsymbol{D}, \tilde{p}_i) + \frac{1}{2}\sigma_{p,i}^2 F_i^2(\tilde{p}_i) \right]. \tag{12}$$

## 4 RESULTS

Since most sources are distributed in the azimuthal range of $-20^\circ < \phi < 60^\circ$, the solar peculiar velocity $\boldsymbol{v}_\odot$ has a non-negligible impact on constraining the rotation shape. Thus we fix the values for $\boldsymbol{v}_\odot$ whose components are $(11.1,\, 12.24,\, 7.25)\,\mathrm{km\ s^{-1}}$ (Schönrich et al. 2010).

Since we focus on elliptical distortion in the Milky Way's rotation, the value of $\alpha$ in the KT94 model should be fixed in our analysis. The radial gradient of the rotation speed has been found to be nearly zero in the solar neighborhood (Zhu 2008, Bovy et al. 2012, Reid et al. 2014). In this case we choose $\alpha = 0$ to constrain the two-dimensional rotation and analyze the stellar motions.

### 4.1 Non-Axisymmetric Rotation Curve Based on the KT94 Model

In the first place, the value of $R_0$ is fixed to be $8.33\,\mathrm{kpc}$ (Gillessen et al. 2009), which was derived from stellar orbits around the massive black hole in the center of the Milky Way. We employ a Markov Chain Monte Carlo method (Metropolis et al. 1953, MCMC) to determine the best-fitting parameters for the KT94 model from the likelihood function in Equation (12).

The estimated parameters are listed in Table 1, where we also give the results in the cases of $\alpha = -0.1$ and $\alpha = 0.1$ as a comparison. The results of $\epsilon_0$ and $\phi_b$ are deduced from $s_0$ and $c_0$. The orbital ellipticity at $R = R_0$, $\epsilon_0$, is significant for all the cases with a value $\gtrsim 0.09$. The azimuth of the minor axis of the elliptical potential (the major axis of the orbit) is at a level of $30^\circ$.

In the work of Metzger et al. (1998), the authors exploited data on Cepheids and investigated the asymmetric component of ellipticity $s_0$, by fixing the symmetric ellipticity $c_0 = 0$. They found $s_0 \sim 0.004 - 0.071$, relying on varying $p$ and $\alpha$. The corresponding $V_0$ changes from around $197\,\mathrm{km\ s^{-1}}$ to around $293\,\mathrm{km\ s^{-1}}$. Fixing $c_0 = 0$ led to systematic bias in the final results, and it is beyond doubt that the determined period-luminosity relation introduced additional uncertainties to the derived kinematical parameters. As for an open cluster, which is another kind of good tracer for the Milky Way's rotation shape, Zhu (2008) divided the sample into different

**Table 1** Kinematical parameters describing elliptical rotation based on the KT94 model with $\alpha = -0.1$, $\alpha = 0$ and $\alpha = 0.1$. The Galactocentric distance of the Sun is assumed to be $8.33\,\mathrm{kpc}$.

| $\alpha$ | $p$ | $V_0$ ($\mathrm{km\,s^{-1}}$) | $s_0$ ($\times 10^{-2}$) | $c_0$ ($\times 10^{-2}$) | $\Delta$ ($\mathrm{km\,s^{-1}}$) | $\epsilon_0$ ($\times 10^{-2}$) | $\phi_b$ ($^\circ$) |
|---|---|---|---|---|---|---|---|
| $-0.1$ | $-1.73 \pm 0.21$ | $259.1 \pm 5.8$ | $10.5 \pm 1.4$ | $5.6 \pm 1.9$ | $9.23 \pm 0.51$ | 11.9 | 30.9 |
| 0 | $0.14 \pm 0.19$ | $235.0 \pm 6.7$ | $8.8 \pm 1.7$ | $2.5 \pm 1.8$ | $10.11 \pm 0.65$ | 9.1 | 37.1 |
| 0.1 | $0.66 \pm 0.18$ | $220.1 \pm 7.9$ | $9.2 \pm 2.1$ | $6.2 \pm 2.0$ | $9.70 \pm 0.40$ | 11.1 | 27.9 |

**Table 2** Correlation coefficients between parameters in the KT94 model in the case of $\alpha = 0$.

| | $p$ | $V_0$ | $s_0$ | $c_0$ | $\Delta$ |
|---|---|---|---|---|---|
| $p$ | 1 | $-0.33$ | $-0.03$ | $-0.08$ | $+0.09$ |
| $V_0$ | | 1 | $-0.37$ | $-0.44$ | $+0.02$ |
| $s_0$ | | | 1 | $+0.18$ | $-0.07$ |
| $c_0$ | | | | 1 | $+0.00$ |
| $\Delta$ | | | | | 1 |

age ranges and estimated the values of $\epsilon_0$ and $\phi_b$. For open clusters younger than 50 Myr, the estimated parameters are $\epsilon_0 = 0.054 \pm 0.013$ and $\phi_b = 29.5^\circ \pm 3.3^\circ$, while the behavior of older open clusters suggests a slightly smaller ellipticity $\epsilon_0 = 0.047 \pm 0.023$ and a major axis (of the orbit) slightly closer to the Sun, i.e. $\phi_b = 27.7^\circ \pm 7.7^\circ$. Since the measured Cepheids and open clusters are mostly confined to the solar neighborhood, the model parameters describing the elliptical rotation, namely ($p$, $V_0$, $s_0$, $c_0$) or ($p$, $V_0$, $\epsilon_0$, $\phi_b$), are difficult to constrain at the same time. Sampling the maser sources, we can obtain estimates of $p$, $V_0$, $s_0$ and $c_0$ simultaneously. The rotation ellipticity traced by masers is $\sim 0.04$ larger than that traced by Cepheids or open clusters. Nonetheless, the major axis of the orbit is verified to be close to the Sun, which indicates that stars in the solar vicinity are moving outward to the apocenter. The $R$- and $\phi$-direction rotation velocities at the location of the Sun are around $22\,\mathrm{km\,s^{-1}}$ and $229\,\mathrm{km\,s^{-1}}$ respectively in the case of $\alpha = 0$. The left panel of Figure 2 presents the residual map based on the $\alpha = 0$ model. The radial and azimuthal residual velocities are shown in the left panel of Figure 3 as functions of $R$.

Table 2 gives the correlation coefficients between the estimated parameters in the $\alpha = 0$ model, which tells us that the correlation between $V_0$ and $c_0$ is the strongest. The degeneracy between $V_0$ and $c_0$ is clearly shown in Figure 4, which is attributed to limited azimuthal coverage of data. More tracers at different azimuths and radii will break the degeneracy between parameters.

### 4.2 Kinematical Calibration of $R_0$

In the above analysis, we fixed the Galactocentric distance to be $R_0 = 8.33\,\mathrm{kpc}$. It is noteworthy that the value of $R_0$ is still debatable. On the one hand, measuring the trigonometric parallax of Sgr B2, a massive star-forming region in the GC, Reid et al. (2009) reported an estimate of $7.9^{+0.8}_{-0.7}\,\mathrm{kpc}$. On the other hand, fitting kinematic data of sampled tracers to a chosen rotation model, the constraint of $R_0$ varies from around 7 kpc to nearly 9 kpc (Shen & Zhu 2007, Gillessen et al. 2009, McMillan & Binney 2010, Schönrich 2012, Bobylev 2013, Matsunaga et al. 2013, Reid et al. 2014, Pietrukowicz et al. 2015, Boehle et al. 2016). In most cases, the kinematical ways of constraining $R_0$ have been based on an assumption that the Milky Way's rotation is circular. In this work, considering the globally non-axisymmetric nature of the Galactic disk, we make a kinematical calibration of $R_0$ using an iteration method, given a prior for the model parameter $p$. Fixing the parameter $p$ obtained by adopting an initial value of $R_0$ (see Table 1), we determine a new estimate of $R_0$. Then using the new $R_0$ as a fixed parameter, a new estimate of $p$ can be derived. The iteration is repeated until convergence is achieved. For each case ($\alpha = -0.1$, $\alpha = 0$ or $\alpha = 0.1$), we have changed the initial value of $R_0$ from 6.7 to 8.9 kpc (McMillan & Binney 2010) and found all these initial values converge to a consistent final solution. The final results are listed in Table 3. The residual map derived from the parameters in the case of $\alpha = 0$ is presented in the right panel of Figure 2. The radial and azimuthal residual velocities along with $R$ (deduced from the new estimate of $R_0$) are plotted in the right panel of Figure 3.

Our results for $R_0$ yielded using the KT94 model are basically coincident with the estimates in Metzger et al. (1998), which gave $R_0 \sim 7.45 - 7.83\,\mathrm{kpc}$. Generally, in order to availably constrain $R_0$ on the basis of a rotation model, we need astrometric data of bright young objects such as masers, OB-type stars, open clusters, classical Cepheids, etc., which are located near the Galactic

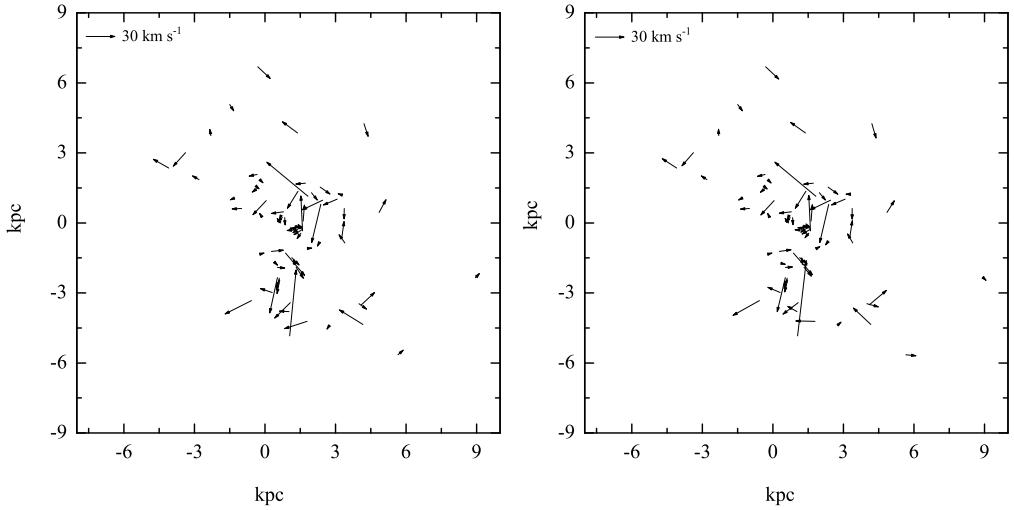


**Fig. 2** Residual velocities of the 70 maser sources projected on the Galactic plane for the KT94 model in the case of $\alpha = 0$. The Sun is located at $(0,\ 0)$. The horizontal coordinate increases towards the direction of Galactic rotation and the vertical coordinate increases towards the Galactic anticenter. The *left panel* is based on the parameters constrained in the case of $R_0 = 8.33\,\mathrm{kpc}$ (see the second row of Table 1); the *right panel* is based on the parameters when $R_0$ is derived as $7.63\,\mathrm{kpc}$ using an iteration method (see the second row of Table 3).

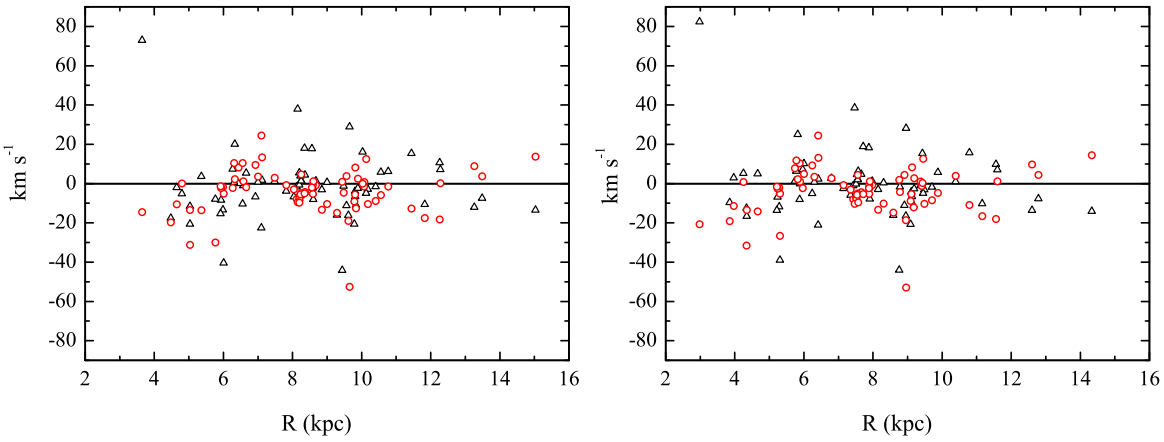


**Fig. 3** Radial (*black triangles*) and azimuthal (*red circles*) residual velocities versus $R$ for the KT94 model in the case of $\alpha = 0$. The *left panel* is based on parameters constrained in the case of $R_0 = 8.33\,\mathrm{kpc}$ (see the second row of Table 1); the *right panel* is based on parameters when $R_0$ is derived as $7.63\,\mathrm{kpc}$ using an iteration method (see the second row of Table 3).

plane and have small dispersions in the velocity field. It is well-known that new-born stars in the cold disk generally reside in the spiral arms, which means that the spiral structure could cause the regional rotation orbit of these stars to deviate. Nonetheless, the elliptical rotation of the Milky Way is thought to be caused by the influence of the central bar or the triaxial halo, thus all the objects that feel the same gravitational potential cannot avoid being affected by the non-axisymmetry of the Galaxy's potential. In our estimation for $R_0$, we focus on the global rotation of the disk and assume that all the sampled tracers rotate around the GC in the potential formulated by KT94. In this case, the value of $R_0$ can be constrained tightly thanks to the widely distributed maser tracers.

## 5 DISCUSSION

The prolate or triaxial structures in the Galaxy (e.g. the bar, bulge and triaxial halo) could dominate the distor-

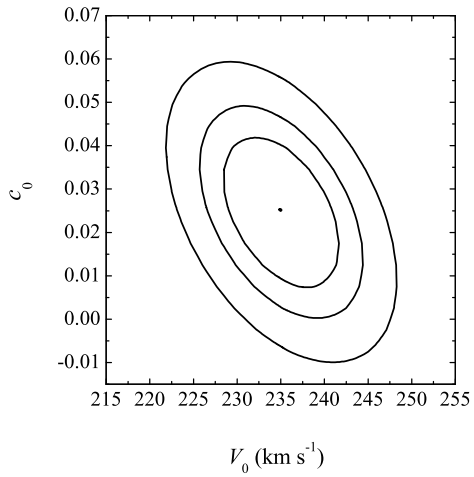


**Fig. 4** Contours of the log-likelihood function projected in the $(V_0,\, c_0)$-plane for the KT94 model in the case of $\alpha = 0$. Contours are drawn at constant log-likelihood values differing from the maximum: $\Delta L = 0.5,\ 1$ and 2, respectively.

**Table 3** Galactic Parameters Calibrated by the KT94 Model

| $\alpha$ | $p$ | $R_0$ (kpc) | $V_0$ (km s$^{-1}$) | $s_0$ ($\times 10^{-2}$) | $c_0$ ($\times 10^{-2}$) | $\Delta$ (km s$^{-1}$) | $\epsilon_0$ ($\times 10^{-2}$) | $\phi_b$ ($^\circ$) |
|---|---|---|---|---|---|---|---|---|
| $-0.1$ | $-2.33$ | $7.64 \pm 0.37$ | $242 \pm 12$ | $7.7 \pm 1.4$ | $5.1 \pm 1.6$ | $9.60 \pm 0.66$ | 9.2 | 28.1 |
| 0 | 0.20 | $7.63 \pm 0.34$ | $215 \pm 10$ | $8.1 \pm 2.0$ | $3.9 \pm 2.0$ | $9.81 \pm 0.69$ | 9.0 | 32.1 |
| 0.1 | 0.96 | $7.13 \pm 0.33$ | $192.2 \pm 8.8$ | $4.8 \pm 1.6$ | $6.4 \pm 1.2$ | $9.96 \pm 0.67$ | 8.0 | 18.3 |

**Table 4** Best-fitting parameters derived from sources residing in the Sagittarius (Sgr) Arm, the Local (Loc) Arm and the Perseus (Per) Arm in the case of $\alpha = 0$, $p = 0.2$. The value of $R_0$ is adopted as 7.63 kpc.

| Spiral arm | $V_0$ (km s$^{-1}$) | $s_0$ ($\times 10^{-2}$) | $c_0$ ($\times 10^{-2}$) | $\Delta$ (km s$^{-1}$) | $\epsilon_0$ ($\times 10^{-2}$) | $\phi_b$ ($^\circ$) |
|---|---|---|---|---|---|---|
| Sgr | $212.8 \pm 8.4$ | $4.3 \pm 2.2$ | $5.1 \pm 2.0$ | $7.2 \pm 1.7$ | 6.7 | 20.1 |
| Loc | $197.7 \pm 9.3$ | $8.5 \pm 2.2$ | $3.4 \pm 2.2$ | $7.61 \pm 0.96$ | 9.2 | 34.2 |
| Per | $230 \pm 14$ | $7.4 \pm 2.4$ | $3.8 \pm 2.2$ | $13.4 \pm 1.6$ | 8.3 | 31.4 |

tion of the Galaxy's potential. Introducing a first-order non-axisymmetric rotation model, we have reconstructed the rotation curve of the Milky Way and calibrated the Galactocentric distance of the Sun.

In our analysis, we focus on the global kinematical feature of the Milky Way. It is noteworthy that the spiral structure could also introduce some bias in the rotation since stars participate in both the global rotation of the Milky Way and the specific motion of the arm in which they reside. In order to compare the kinematics of different arms, we select 12, 23 and 18 sources from the Sagittarius, Local and Perseus Arms and explore their rotations respectively. We assume $\alpha = 0$ for each of the arms. The values of $p$ and $R_0$ are fixed at 0.2 and 7.63 kpc respectively, coming from the estimation in Section 4.2. Table 4 lists the best-fitting parameters derived from different arms. Figure 5 presents the modeled rotation velocities as functions of azimuths for each arm.

It is clear that the rotation of each single arm deviates from being circular and there are notable discrepancies among the rotation properties of different arms. The rotation ellipticity of the Sagittarius Arm is $\gtrsim 0.02$ smaller than that of the Local and Perseus Arms, and the azimuth of the major axis of the Sagittarius Arm's orbit is also $\gtrsim 10^\circ$ smaller than those of the other two arms. Although the Local and Perseus Arms share similar rotation shapes, it is worth noting that the velocity dispersion of sources residing in the Perseus Arm is much larger than that in the other two arms. The total velocity dispersion derived from the Perseus sources is approximately $10\,\mathrm{km\,s^{-1}}$ larger than that from the bluest stars in the *Hipparcos* catalog (Dehnen & Binney 1998; Aumer &

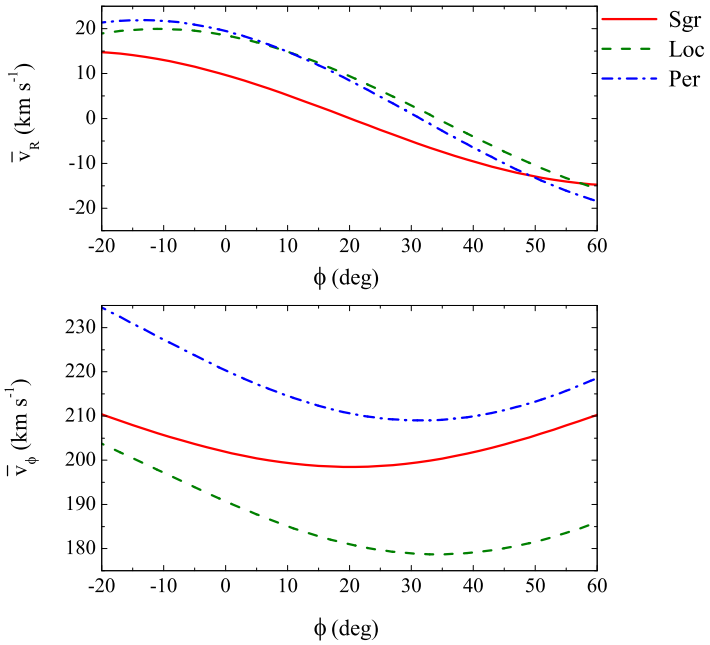


**Fig. 5** Model velocities along the azimuth obtained from the best-fitting kinematical parameters in Table 4. The *red solid line*, *olive dashed line* and *blue dash-dotted line* represent velocities of the Sagittarius (Sgr), Local (Loc), and Perseus (Per) Arms respectively. For each arm the Galactocentric distance is fixed at the sample mean $\langle R \rangle$ of all the sources residing in it: $\langle R \rangle = 6.0\,\mathrm{kpc}$, $7.7\,\mathrm{kpc}$, $9.4\,\mathrm{kpc}$ for Sagittarius, Local and Perseus Arms respectively. The *upper panel* shows the radial velocities $\bar{v}_R$ and the *lower panel* shows the azimuthal velocities $\bar{v}_\phi$.

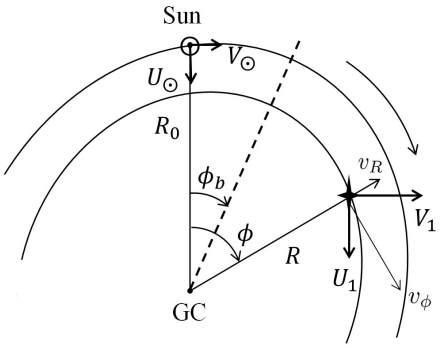


**Fig. 6** Orbits of the Sun and the source in the Galactic plane for an assumed elliptical rotation. $R_0$ and $R$ are the Galactocentric distances of the Sun and the source respectively. $\phi_b$ and $\phi$ are the azimuths of the major axis of the orbit and the source respectively. $v_R$ and $v_\phi$ denote the velocities in the directions of increasing $R$ and $\phi$. $U_1$ and $V_1$ indicate the velocities relative to the Sun in the heliocentric Cartesian coordinate system in the directions $u$ and $v$ respectively. $U_\odot$ and $V_\odot$ denote the solar peculiar motions.

Binney 2009). Such significant peculiar motions in the Perseus Arm could be attributed to several causes. First, the heating process in the Perseus Arm could be more violent than in the other two arms, but there is no evidence that the Perseus Arm is obviously warmer than the others. Second, the large peculiar motions of Perseus sources could be attributed to the probable interaction between the outer disk and the halo (Normandeau et al. 1996; Levine et al. 2006), but it is doubtful whether the halo could act significantly on the new-born stars. Third, the random motions of stars in the Perseus Arm might not satisfy Gauss' law. For the simplest case we adopt an isotropous Gaussian distribution for the random component of stellar velocities in all the arms, but the Gaussian distribution may have limitations when describing kinematics of the Perseus Arm and there could be some unmodeled motions for the Perseus stars. Theoretically, a higher-order rotation model with more parameters could

describe the stellar velocities in more detail, but the reliability of the constrained parameters in a more complex model undoubtedly depends on the sample completeness. A spiral arm is one of the dominant structures in the Galactic disk, and masers are good tracers of arm kinematics. A more homogenous spatial distribution of observed masers will help us construct a detailed kinematical model for a spiral arm.

In this work we investigate kinematical non-axisymmetry in the $(R,\,\phi)$-plane under an assumption that the equipotential surfaces of the Galaxy's potential are approximately elliptical. By exploiting maser data, a weak potential ellipticity of $\epsilon_0 \sim 0.09$ is detected. It is worth noting that there still exist some unknowns in stellar motions. On the one hand, regional distortions such as the distortion caused by Galactic warp or spiral waves (Miyamoto & Zhu 1998; Bobylev 2010; Bobylev & Bajkova 2015a) could increase the complexity of the stellar velocity field. On the other hand, the motion of masers suggests a larger ellipticity than that of later-type thin-disk objects (e.g. open clusters and Cepheids). More complete data on tracers will help us to explore the Galactic kinematics over different scales.

## 6 SUMMARY

The Milky Way's rotation can be distorted into an ellipse by the non-axisymmetric potential of the Galaxy. In this work we describe the shape of the Milky Way's rotation using a non-axisymmetric rotation model formulated by KT94. Employing and generalizing the ML method formulated by AL13, we exploit the data thoroughly and analyze the elliptical rotation of our home galaxy traced by maser sources selected from Reid et al. (2014).

The power-law index of the radius-dependent non-axisymmetric part of the Galaxy's potential, $p$, is estimated to be $\sim 0.20$, coupled with a potential ellipticity $\sim 0.09$ at the Sun, and the minor axis of the elliptical potential (the major axis of the orbit) is found to be near the Sun with a displacement $\sim 32^\circ$. Based on the KT94 model, we deal with a kinematical calibration of the Galactocentric distance of the Sun. An estimated value of $7.63 \pm 0.34\,\mathrm{kpc}$ is obtained in the final solution.

**Acknowledgements** This work is funded by the National Natural Science Foundation of China (NSFC) under grant Nos. 11303018 and 11473013 and the Natural Science Foundation of Jiangsu Province under No. BK20130546. We wish to thank the anonymous referee for useful comments and suggestions which helped to improve the manuscript.

### Appendix A:

In order to obtain the expressions of $\boldsymbol{v}$ and $\boldsymbol{D_v}$ in Section 3.2, we define heliocentric velocities $U_1$, $V_1$ and $W_1$ to be the velocities relative to the Sun in the three directions $u$, $v$ and $w$ in the heliocentric Cartesian coordinate system, respectively (see Fig. 6). In this case, $(U_1,\,V_1,\,W_1)$ can be calculated via

$$\begin{pmatrix} U_1 \\ V_1 \\ W_1 \end{pmatrix} = M_1 \begin{pmatrix} v_R \\ v_\phi \\ v_z \end{pmatrix} + \begin{pmatrix} +v_{R,(R=R_0,\,\phi=0^\circ)} \\ -v_{\phi,(R=R_0,\,\phi=0^\circ)} \\ 0 \end{pmatrix} - \boldsymbol{v}_\odot, \tag{A.1}$$

where $M_1$ is a $3 \times 3$ matrix

$$\boldsymbol{M}_1 = \begin{pmatrix} -\cos\phi & \sin\phi & 0 \\ \sin\phi & \cos\phi & 0 \\ 0 & 0 & 1 \end{pmatrix} \tag{A.2}$$

that projects any vector from the Galactocentric cylindrical coordinate system to the heliocentric Cartesian coordinate system. Now the values of $\boldsymbol{v}$ can be obtained from $(U_1,\,V_1,\,W_1)$

$$\boldsymbol{v} = M_2 \begin{pmatrix} U_1 \\ V_1 \\ W_1 \end{pmatrix}, \tag{A.3}$$

where $M_2$ is a $3 \times 3$ matrix

$$\boldsymbol{M}_2 = \begin{pmatrix} -\sin l & \cos l & 0 \\ -\sin b\cos l & -\sin b\sin l & \cos b \\ \cos b\cos l & \cos b\sin l & \sin b \end{pmatrix}. \tag{A.4}$$

Finally the covariance of $\boldsymbol{D_v}$ resulting from the dispersion tensor $\boldsymbol{D}$ is in the following form

$$\boldsymbol{D_v} = \boldsymbol{M_2 M_1 D {M_1}^{\mathrm{T}} {M_2}^{\mathrm{T}}}. \tag{A.5}$$

## References

Aghajani, T., & Lindegren, L. 2013, A&A, 551, A9
Aumer, M., & Binney, J. J. 2009, MNRAS, 397, 1286
Binney, J. 1978, MNRAS, 183, 779
Blitz, L., & Spergel, D. N. 1991, ApJ, 370, 205
Bobylev, V. V. 2010, Astronomy Letters, 36, 634
Bobylev, V. V. 2013, Astronomy Letters, 39, 95
Bobylev, V. V., & Bajkova, A. T. 2015a, MNRAS, 447, L50
Bobylev, V. V., & Bajkova, A. T. 2015b, Astronomy Letters, 41, 473

Bobylev, V. V., & Bajkova, A. T. 2017, Astronomy Letters, 43, 159
Boehle, A., Ghez, A. M., Schödel, R., et al. 2016, ApJ, 830, 17
Bovy, J., Allende Prieto, C., Beers, T. C., et al. 2012, ApJ, 759, 131
Chemin, L., Renaud, F., & Soubiran, C. 2015, A&A, 578, A14
de Vaucouleurs, G. 1970, in IAU Symposium, 38, The Spiral Structure of our Galaxy, eds. W. Becker & G. I. Kontopoulos, 18
Dehnen, W., & Binney, J. J. 1998, MNRAS, 298, 387
Dwek, E., Arendt, R. G., Hauser, M. G., et al. 1995, ApJ, 445, 716
Elias, F., Alfaro, E. J., & Cabrera-Caño, J. 2006, AJ, 132, 1052
Gerhard, O. 2016, in IAU Symposium, 317, The General Assembly of Galaxy Halos: Structure, Origin and Evolution, eds. A. Bragaglia, M. Arnaboldi, M. Rejkuba, & D. Romano, 266
Gillessen, S., Eisenhauer, F., Trippe, S., et al. 2009, ApJ, 692, 1075
Huang, Y., Liu, X.-W., Yuan, H.-B., et al. 2016, MNRAS, 463, 2623
Kuijken, K. 1996, in Astronomical Society of the Pacific Conference Series, 91, IAU Colloq. 157: Barred Galaxies, eds. R. Buta, D. A. Crocker, & B. G. Elmegreen, 504
Kuijken, K., & Tremaine, S. 1994, ApJ, 421, 178
Levine, E. S., Blitz, L., Heiles, C., & Weinberg, M. 2006, astro-ph/0609554
Lindegren, L., Lammers, U., Bastian, U., et al. 2016, A&A, 595, A4
López-Corredoira, M. 2014, A&A, 563, A128
López-Corredoira, M., & González-Fernández, C. 2016, AJ, 151, 165
Matsunaga, N., Feast, M. W., Kawadu, T., et al. 2013, MNRAS, 429, 385
McMillan, P. J., & Binney, J. J. 2010, MNRAS, 402, 934
Metropolis, N., Rosenbluth, A. W., Rosenbluth, M. N., Teller, A. H., & Teller, E. 1953, J. Chem. Phys., 21, 1087
Metzger, M. R., Caldwell, J. A. R., & Schechter, P. L. 1998, AJ, 115, 635
Miyamoto, M., & Zhu, Z. 1998, AJ, 115, 1483
Normandeau, M., Taylor, A. R., & Dewdney, P. E. 1996, Nature, 380, 687
Pietrukowicz, P., Kozłowski, S., Skowron, J., et al. 2015, ApJ, 811, 113
Reid, M. J. 2012, in IAU Symposium, 287, Cosmic Masers - from OH to H0, eds. R. S. Booth, W. H. T. Vlemmings, & E. M. L. Humphreys, 359
Reid, M. J., & Dame, T. M. 2016, ApJ, 832, 159
Reid, M. J., Menten, K. M., Brunthaler, A., et al. 2014, ApJ, 783, 130
Rojas-Niño, A., Martínez-Medina, L. A., Pichardo, B., & Valenzuela, O. 2015, ApJ, 805, 29
Schönrich, R. 2012, MNRAS, 427, 274
Schönrich, R., Binney, J., & Dehnen, W. 2010, MNRAS, 403, 1829
Sharma, S., Bland-Hawthorn, J., Binney, J., et al. 2014, ApJ, 793, 51
Shen, M., & Zhu, Z. 2007, ChJAA (Chin. J. Astron. Astrophys.), 7, 120
Uemura, M., Ohashi, H., Hayakawa, T., et al. 2000, PASJ, 52, 143
Zhu, Z. 2006, ChJAA (Chin. J. Astron. Astrophys.), 6, 363
Zhu, Z. 2008, ChJAA (Chin. J. Astron. Astrophys.), 8, 96